Nucleic Acids Research, 1997, Vol. 25, No. 10 **1943–1949**

A mutant RNA pseudoknot that promotes ribosomal frameshifting in mouse mammary tumor virus

Hunseung Kang[+] and Ignacio Tinoco Jr*

Department of Chemistry, University of California, Berkeley and Structural Biology Division, Lawrence Berkeley National Laboratory, Berkeley, CA 94720-1460, USA

Received January 28, 1997; Revised and Accepted March 27, 1997

ABSTRACT

A single A→G mutation that changes a potential A·U base pair to a G·U pair at the junction of the stems and loops of a non-frameshifting pseudoknot dramatically increases its frameshifting efficiency in mouse mammary tumor virus. The structure of the non-frameshifting pseudoknot APK has been found to be very different from that of pseudoknots that cause efficient frameshifting [Kang,H., Hines,J.V. and Tinoco,I. (1995) *J. Mol. Biol.*, 259, 135–147]. The 3-dimensional structure of the mutant pseudoknot was determined by restrained molecular dynamics based on NMR-derived interproton distance and torsion angle constraints. One striking feature of the mutant pseudoknot compared with the parent pseudoknot is that a G·U base pair forms at the top of stem 2, thus leaving only 1 nt at the junction of the two stems. The conformation is very different from that of the previously determined non-frameshifting parent pseudoknot, which lacks the A·U base pair at the top of the stem and has 2 nt between the stems. However, the conformation is quite similar to that of efficient frameshifting pseudoknots whose structures were previously determined by NMR. A single adenylate residue intervenes between the two stems and interrupts their coaxial stacking. This unpaired nucleotide produces a bent structure. The structural similarity among the efficient frameshifting pseudoknots indicates that a specific conformation is required for ribosomal frameshifting, further implying a specific interaction of the pseudoknot with the ribosome.

INTRODUCTION

Retroviruses use ribosomal frameshifting to synthesize essential viral enzymes, reverse transcriptase, protease and integrase, from a single polycistronic messenger RNA (1,2). An RNA pseudoknot located downstream of the heptanucleotide shift site plays an important role in this frameshifting event. The mechanism by which pseudoknot-induced ribosomal frameshifting occurs is not yet understood. It has been proposed that a pseudoknot induces frameshifting by hindering the approaching ribosome and making it stall or pause at the shift site. This pausing is thought to contribute to the probability of a reading frame shift into the –1 frame (3,4).

However, in a recent mutational study, Chen *et al.* (5) showed that the frameshifting abilities of RNA pseudoknots in mouse mammary tumor virus (MMTV) dramatically change depending on single base substitutions at the junction of the stems and loops of the pseudoknot. Frameshifting was not simply related to the free energy of the pseudoknot. This indicates that specific structural features rather than stability alone of the RNA pseudoknot are involved in promoting efficient ribosomal frameshifting.

The structures of two efficient and two poor frameshifting pseudoknots were determined by NMR (6–8). The efficient frameshifting pseudoknots adopt a characteristic bent conformation, which is very different from that of the non-frameshifting pseudoknots. Based on these NMR and mutational studies, we proposed that a pseudoknot is not a simple energetic barrier to an approaching ribosome, but that there is a specific interaction between pseudoknot and ribosome or ribosome-related factors (8).

To address this hypothesis more clearly, the structures of other pseudoknots with different frameshifting efficiencies need to be studied. Here we present the 3-dimensional structure of a mutant RNA pseudoknot from MMTV. This pseudoknot, designated APKA27G in Figure 1, has a single A27→G27 base substitution in the parent pseudoknot APK. The frameshifting efficiency of this mutant pseudoknot APKA27G is four times higher than that of the parent pseudoknot APK (8 versus 2%). We show that APKA27G adopts structural features similar to those of the efficient frameshifting pseudoknot VPK (6). This result further supports the hypothesis that a characteristic bent pseudoknot is recognized by the ribosome or ribosome-related factors and that this promotes efficient frameshifting in MMTV.

MATERIALS AND METHODS

RNA synthesis and purification

Oligoribonucleotides were synthesized *in vitro* from DNA templates using T7 RNA polymerase (9,10). RNA oligonucleotides were purified by 20% PAGE under denaturing conditions (7 M urea). The RNA transcripts were visualized by UV shadowing, excised, electroeluted from the gel (Schleicher & Schuell Co.) and precipitated with ethanol. UV melting studies were done to verify

*To whom correspondence should be addressed. Tel: +1 510 642 3038; Fax: +1 510 643 6232; Email: intinoco@lbl.gov

[+]Present address: Kumho Life and Environmental Science Laboratory, Sangamdong, Kwangsangu, Kwanju, Korea

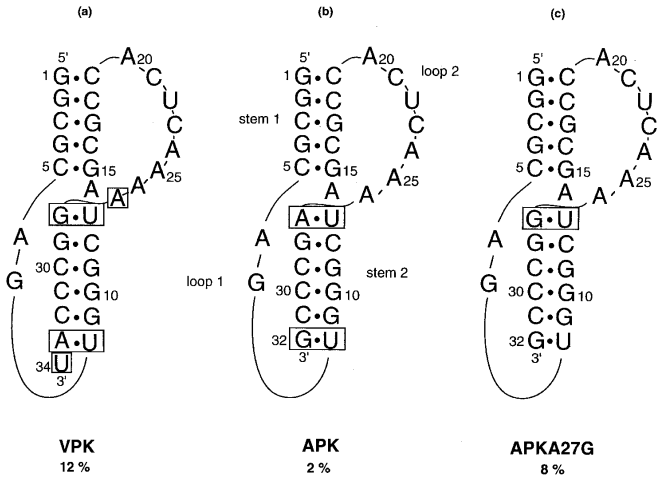

Figure 1. Comparison of sequences and frameshifting efficiencies of the RNA pseudoknots; the boxed nucleotides differ among the different pseudoknots. (**a**) Pseudoknot VPK promotes efficient ribosomal frameshifting in MMTV (6). (**b**) Pseudoknot APK is fomed from VPK by deleting A27; changing G28·U13 to A·U and deleting A33·U8 and U34. APK does not promote efficient frameshifting (7). (**c**) The mutant pseudoknot APKA27G, examined in this study, has a single A27→G27 substitution in APK and promotes efficient frameshifting. The frameshifting efficiencies in percent are given below each structure. Frameshifting assays were done in rabbit reticulocytes as described in our earlier studies (5–8).

that the folded structures formed were monomeric even at high strand concentrations. The secondary structures of the RNA oligonucleotides were probed using nucleases S1, T1 and V1 (11).

NMR experiments

All NMR spectra were obtained on a GE GN-500 or a Bruker AMX-600 spectrometer. The purified RNA was first dialyzed extensively against 10 mM sodium phosphate, pH 7.0, 100 mM NaCl, 5 mM EDTA and then against 10 mM sodium phosphate, pH 6.4, 50 mM NaCl. After dialysis, 0.2 M $MgCl_2$ was added to the sample to a final concentration of 5 mM. All measurements were made at 25°C, unless otherwise specified. Samples used in exchangeable proton experiments were prepared by adding a 10:1 mixture of H_2O and D_2O to dry RNA. For non-exchangeable proton experiments, RNA was lyophilized several times with 99.9% D_2O in the NMR tube and finally dissolved in 0.22 ml 99.96% D_2O (Aldrich) to a final concentration of ~2 mM.

1-Dimensional (1D) exchangeable proton spectra were taken on a GE GN-500 using a 1-1 sequence for solvent suppression (12) with 12 000 Hz spectral width. The excitation maximum was set between the imino and aromatic resonance regions.

All 2-dimensional (2D) NMR spectra were recorded in the phase-sensitive mode using the TPPI method (13) and pre-irradiation of the residual HDO peak. Typically, 2000 complex points in t_2 and 370–450 FIDs in t_1 were collected with spectral widths of 4700–5000 Hz. The total relaxation delay was 2.5 s. Data were processed using FELIX (Biosym Technologies Inc.) on a Silicon Graphics IRIS workstation.

NOESY spectra in D_2O were recorded with mixing times of 60, 100, 150 and 300 ms. Data were zero-filled to 2000 real points in t_1 and were apodized by using phase-shifted sine bells in both dimensions. NOESY spectra in H_2O were recorded with a spectral width of 12 000 Hz and a mixing time of 300 ms. Spectra were obtained at 10°C with a 1-1 water suppression sequence replacing the last pulse (12). Approximately 370 FIDs of 2000 complex points were collected.

Double quantum-filtered COSY (DQF-COSY) spectra were collected using the pulse sequence with composite mixing pulses (14). For high resolution DQF-COSY, broad band phosphorus decoupling was achieved by GARP1 (15) and a narrow spectral width (2000 Hz) was used for 4000 complex data points. A total of 712 FIDs was collected with 32 scans.

Total correlation spectroscopy (TOCSY) experiments were acquired using a MLEV-17 for broad band decoupling (16), with a long mixing time (120 ms) to maximize relayed magnetization transfer from the H1′ protons to the other sugar protons.

Natural abundance ^{13}C–^{1}H heteronuclear multiple quantum correlations (HMQC) were recorded at 600 MHz with spectral widths of 20 000 (^{13}C) and 5000 Hz (^{1}H) and GARP1 carbon decoupling during acquisition. Approximately 180–200 FIDs of 2000 complex points were recorded and 256 scans were averaged for each FID.

Interproton distance and torsion angle constraints

The cross-peak intensities in NOESYs at 60, 100 and 150 ms mixing times were evaluated by integrating their volumes using FELIX (Biosym Technologies Inc.). The pyrimidine H5–H6 distance was used as a reference. NOEs were classified into four categories: strong, medium, weak and very weak. The strong and medium cross-peaks were given a distance range of 1.8–3.0 and 2.0–4.0 Å respectively and the weak and very weak cross-peaks were given a distance range of 2.5–5.0 and 3.5–6.0 Å respectively. A total of 263 non-exchangeable proton distance constraints were obtained from the D_2O NOESY spectra. For imino–imino proton distances, a distance range of 3.2–4.5 Å was assigned to the cross-peaks observed in the H_2O NOESY spectra.

The sugar puckers were determined by measuring ^{1}H–^{1}H scalar couplings in phosphorus-decoupled high resolution DQF-COSY. The nucleotides without observable H1′–H2′ couplings were restrained to be C3′-*endo*. The glycosidic torsion angle χ was constrained to be *anti* for nucleotides that do not have strong intranucleotide H8/H6–H1′ NOEs at short mixing time NOESY. In addition to the torsion angles for maintaining correct sugar pucker conformations and for keeping *anti* orientations of the bases relative to the sugars, empirical constraints to keep the amino groups in the planes of the bases were used during global folding of the RNA. During refinement of the pseudoknot structure, backbone torsion angle constraints (α, β, γ, ε and ζ), derived from the standard values for A-form helices (17), were added to the torsion angle constraint file for the base pairs in the stems of the pseudoknot.

Structure determination

The simulated annealing and restrained molecular dynamics (rMD) program X-PLOR (18) was used with experimental distance and torsion angle constraints derived from the NMR data. Thirty starting structures generated using random torsion angles were subjected to two stages of calculation: global fold and refinement. Global folds were calculated using only the repulsive van der Waals term and no electrostatic interactions. Five hundred cycles of initial energy minimization, followed by rMD as the temperature was cooled from 1000 to 300 K, and finally 1000 cycles of energy minimization were performed for the global fold. Structures with

lower total energies and fewer NOE violations from the global fold were subjected to the refinement calculation. This involved: 500 cycles of initial energy minimization, rMD at 1000 K with backbone torsion angle constraints for the stem regions introduced in two steps (β, γ and ε first; α and ζ second) according to Wimberly (19), rMD while cooling to 300 K and 1000 cycles of subsequent energy minimization. The force constant for NOE was set to 50 kcal/mol/Å^2 and the torsion angle force constant was varied between 5 and 50 kcal/mol/rad^2 during the calculations. Finally, 3000 cycles of energy minimization were done for the refined structures with Lennard–Jones potentials and electrostatic energies included.

RESULTS

Assignment of the exchangeable proton resonances

Figure 2 shows the exchangeable proton spectrum of the pseudoknot APKA27G at 15°C. Nine imino resonances from the imino protons in the G·C base pairs of the helical regions of the pseudoknot are observed in the chemical shift region 13.5–12 p.p.m. Sequence-specific assignments of the imino resonances were made from 2D NOESY spectra in H_2O using the procedure of Heus and Pardi (20).

The positions of assigned imino peaks for the pseudoknot APKA27G are similar to those observed for APK (7), except for a down-field shift of the G28 imino proton. A similar shift of the G29 imino proton was also observed for the pseudoknot VPK, where the corresponding G28 residue base pairs with residue U13 (6). This observation indicates that the U13·G27 base pair may form in APKA27G, although the resonance from the U13 imino proton is not visible. This contrasts with APK, where no U13·A27 base pair is formed (7). Formation of the U13·G27 base pair is also supported by several NOEs between G28 and G27 in the D_2O NOESY spectra, a shift of the H5/H6 cross-peak for U13 in the DQF-COSY (Fig. 3), as observed in VPK, and protection of G28 from cleavage by a ribonuclease T1–Ni(II) complex (data not shown).

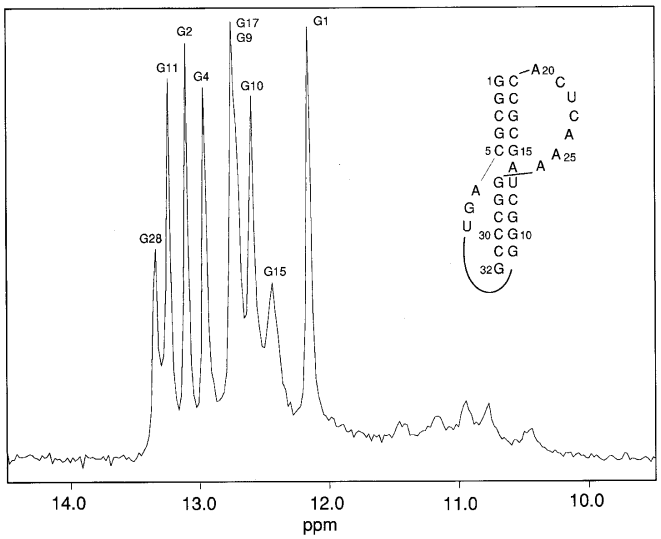

Figure 2. Imino proton spectrum of the pseudoknot APKA27G in 10 mM sodium phosphate, pH 6.4, 50 mM NaCl, 5 mM $MgCl_2$ at 15°C. Assignments of the imino protons were made from a NOESY spectrum.

A possible U8·G32 base pair does not form at the bottom of stem 2. There are no significant changes in the chemical shifts of base and sugar protons of U8, G9 and G32 compared with those for APK and no NOE connectivity between U8 and G9, as observed in APK (7). From these results, we concluded that stem 2 of the pseudoknot APKA27G consists of four G·C base pairs and a G·U base pair. A sharp and up-field shifted imino resonance from G1 is also observed, indicating stacking of residue A20 upon the G1·C19 base pair, as discussed before (6,7,21).

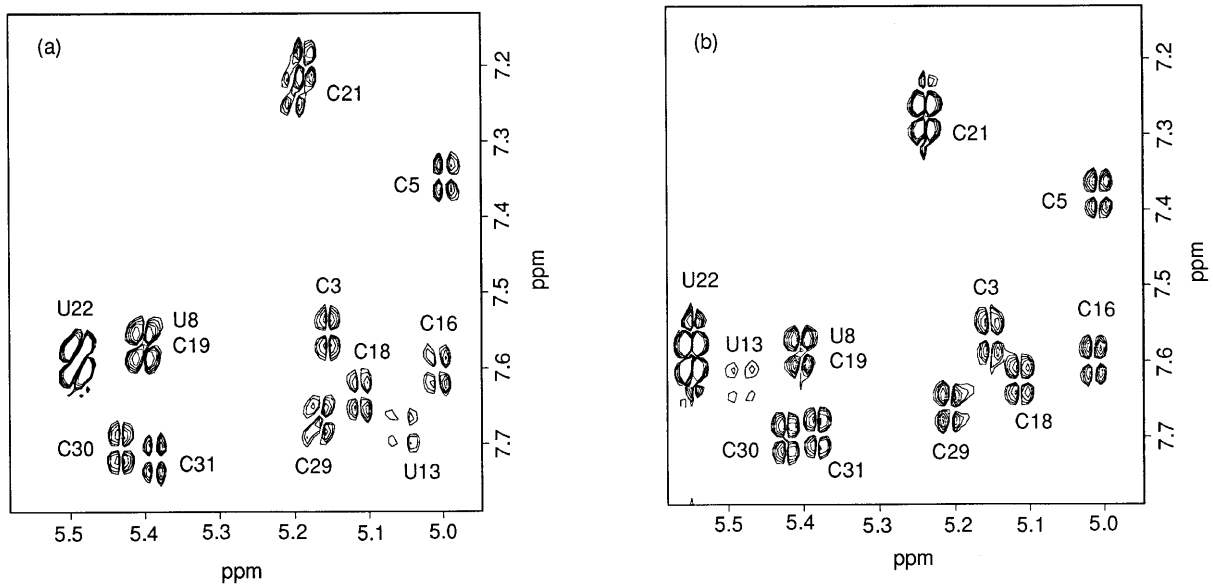

Figure 3. Comparison of a DQF-COSY of (**a**) the mutant pseudoknot APKA27G with that of (**b**) the parent pseudoknot APK in 10 mM sodium phosphate, pH 6.4, 50 mM NaCl, 5 mM $MgCl_2$ at 25°C. Note the large shift of the H5/H6 cross-peak for U13.

Table 1. Chemical shifts (p.p.m.) of non-exchangeable and imino protons for the mutant pseudoknot APKA27G in 10 mM sodium phosphate, pH 6.4, 50 mM NaCl, 5 mM $MgCl_2$ at 25°C.

Residue	H8/H6	H2/H5	H1′	H2′	H3′	Imino[a]
G1	8.25	na	5.85	4.79	4.27	12.17
G2	7.50	na	5.75	4.45	4.53	13.13
C3	7.57	5.14	5.48	4.59		na
G4	7.41	na	5.64	4.47	4.35	12.99
C5	7.38	5.00	5.29	4.42	4.41	na
A6	7.98	8.14	5.83	4.40	4.10	na
G7	7.48	na	5.62	3.82	4.40	
U8	7.59	5.40	5.60	4.13	4.27	
G9	7.99	na	5.66	4.82	4.82	12.75
G10	7.42	na	5.79	4.78	4.70	12.61
G11	6.98	na	5.56	4.34	3.94	13.26
C12	7.44	4.77	5.45	4.56	4.24	na
U13	7.66	5.45	5.65	4.56	4.45	
A14	8.35		5.91	4.47	4.59	na
G15	6.78	na	5.22	4.30	4.26	12.47
C16	7.60	5.00	5.39	4.33	4.27	na
G17	7.49	na	5.61	4.34		12.77
C18	7.63	5.10	5.46	4.38		na
C19	7.58	5.40	5.42	4.52	4.56	na
A20	7.81	7.05	5.79	4.32	4.37	na
C21	7.27	5.25	5.22	3.91	4.21	na
U22	7.59	5.56	5.72	4.26		
C23	7.59	5.87	5.72	4.09	4.44	na
A24	8.16	7.91	5.86	4.73	4.53	na
A25	8.07	7.91	5.75	4.60	4.76	na
A26	8.06		5.81	4.63		na
G27	7.55	na	5.72	4.45	4.74	
G28	7.50	na	5.71	4.52		13.39
C29	7.66	5.21	5.50	4.29	4.50	na
C30	7.68	5.43	5.44	4.31		na
C31	7.70	5.39	5.45	4.38		na
G32	7.55	na	5.67	3.98	4.18	

[a]Measured at 15°C.
na, not applicable.
All chemical shifts are referenced to trimethylsilylpropionate (TSP).

Assignment of the non-exchangeable proton resonances

Basically similar strategies used for the parent pseudoknot APK (7) were employed to assign the non-exchangeable protons for the mutant pseudoknot APKA27G. In the stems, standard aromatic–H1′ sequential NOE connectivities were used to assign aromatic and H1′ resonances. H2′ resonances were assigned from the strongest NOEs to the H1′ protons at a short mixing time (60 ms). H3′ resonances in stems were assigned using NOE connectivities H8/H6(i)–H3′(i)–H1′(i) and further verified by using H8/H6(i+1)–H3′(i) connectivities.

In the loops, NOESY, DQF-COSY and TOCSY spectra were used to assign resonances. Aromatic and H1′ resonances were assigned using aromatic–H1′ NOE connectivities. H2′ resonances were assigned from the strongest NOEs to the H1′ protons at short mixing times (60 ms) just as for the stems. Assignments of the H1′ and H2′ resonances of the loop nucleotides with observable H1′–H2′ scalar couplings were further verified by a DQF-COSY experiment. Finally, a TOCSY experiment was used to confirm previously assigned H2′ and H3′ resonances.

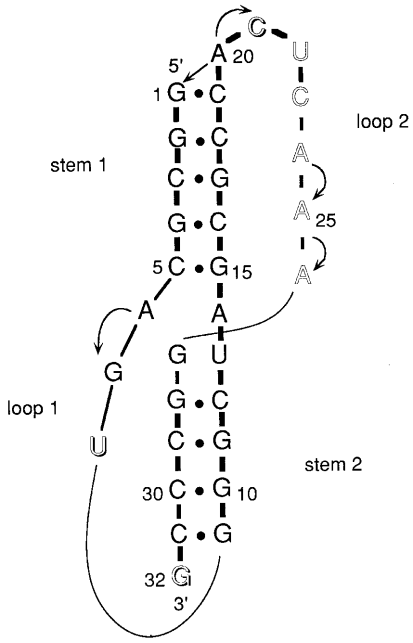

Figure 4. Summary of the NMR data observed for the mutant pseudoknot APKA27G. Internucleotide NOEs are represented by the thickness of each line; thick, medium and thin lines represent more than three NOEs, two or three NOEs and no NOE respectively. Inter-residue AH2–H1′ NOEs are indicated by an arrow. Black dots (•) represent hydrogen bonded imino protons. Sugar conformation is indicated by letter type: bold represents C3′-*endo*, outline represents C2′-*endo* and shadow represents equilibrium between C2′- and C3′-*endo* sugar puckers.

All assignments for the mutant pseudoknot APKA27G were greatly facilitated by comparing the NMR spectra with those for the parent pseudoknot, APK. The spectral assignments of the pseudoknot APKA27G in 10 mM sodium phosphate, pH 6.4, 50 mM NaCl, 5 mM $MgCl_2$ at 25°C are summarized in Table 1.

Structural features of the mutant pseudoknot APKA27G

As summarized in Figure 4, the mutant pseudoknot APKA27G contains structural features that are similar to the parent pseudoknot APK, except for a few major differences. Characteristic A-form stacking interactions are observed in both stems, as seen in APK. Many NOEs were observed between aromatic and sugar protons for the nucleotides at the junction region of stems 1 and 2, indicating continuous stacking of residues C12–G15. However, less and weaker NOEs are observed between A14 and G15 compared with APK. A20, the first nucleotide in loop 2, has a strong NOE from H8 to C19H2′ and a medium NOE from H2 to G1H1′, as well as three other NOEs between A20 aromatic and C19 sugar and aromatic protons. All these NOEs indicate that residues G9–A20 of the pseudoknot APKA27G are continuously stacked, although more distortions from a standard A-form stacking interaction are present at the junction of the two stems than those observed for APK.

In addition to the similar structural features discussed above, APKA27G contains quite different structural features from those of APK. In contrast to the strong stacking in the C5–A6–G7 steps of APK (7), only a weak stacking was observed in the C5–A6 step of APKA27G. No NOEs were observed from A6H2 to G7H1′ and to the cross-strand G15H1′, which are characteristic NOEs of

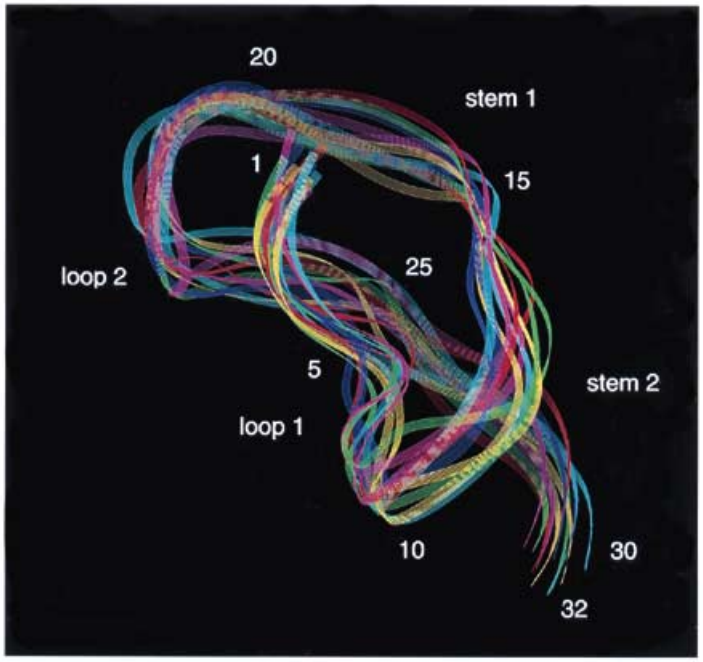

Figure 5. Superimposition of the 12 energy minimized pseudoknot structures based on all atoms. Only the phosphate backbones are shown for clarity and to represent the overall conformations of the pseudoknots.

APK, indicating that the C5–A6–G7 steps are not as strongly stacked as in APK. For stem 2, strong to medium NOEs were observed from H8 of G28 to H2′/H3′ of G27, indicating that G27–G28 is stacked. No NOEs were observed between A26 and G27.

From these NOE results and the down-field shifted G28 imino resonance discussed above, we concluded that the U13·G27 base pair forms. Thus stem 2 of APKA27G consists of four G·C base pairs and a G·U base pair.

Although NOE connectivities of the loop nucleotides deviate from those observed for A-form geometry, as discussed for APK (7), several NOEs from aromatic to sugar protons between neighboring nucleotides were observed for residues C21–A26, indicating that residues in loop 2 are more or less stacked on each other. However, the stacking interactions between nucleotides in loop 2 of APKA27G are much weaker than those of APK.

Scalar coupling (J coupling) information was used to characterize the sugar conformations as C3′-*endo* or C2′-*endo* puckers. Nucleotides in both loops have detectable H1′–H2′ couplings, with 4–5 Hz couplings for U8 in loop 1, C21 in loop 2 and the terminal G32. These intermediate H1′–H2′ coupling constants indicate that these residues are in equilibrium between C2′-*endo* and C3′-*endo* sugar conformations. For U22–A26 in loop 2 ~9 Hz H1′–H2′ couplings were observed, in contrast to the 4–5 Hz couplings for APK, indicating that these nucleotides adopt mainly the C2′-*endo* sugar conformation. Absence of detectable H1′–H2′ couplings for the nucleotides in both stems and loops (e.g. A6, G7 and A20) indicates that these residues adopt the C3′-*endo* sugar pucker, as expected for nucleotides in A-form helices.

Structure determination

Thirty starting structures for the mutant pseudoknot APKA27G were generated by randomizing backbone torsion angles α, β, γ, ε and ζ and with torsion angles δ and χ set to C3′-*endo* and *anti* respectively. In addition to the inter-proton distances and torsion angle constraints deduced from the measured intensities of NOE cross-peaks and H1′–H2′ coupling constants respectively, four additional distance constraints were used to maintain hydrogen bonding for G27·U13 and for each of the nine G·C base pairs in the stems. Therefore, the input data included 263 NOE-based distance restraints, 41 hydrogen bond distances, 16 base pair planarity restraints and 189 torsion angle dihedral restraints. The dihedral restraints were of three kinds: 128 sugar pucker angles, 29 angles to keep amino groups in the plane of the bases and 32 χ angles to keep the bases *anti*. After global folding of the starting structures using a simulated annealing protocol, structures with lower total energy and NOE violations were selected for further refinement. Twelve out of 30 starting structures converged to this lower energy category.

For subsequent refinement calculations, the same NOE restraints file used for global folding was used. The dihedral restraints file, however, was modified for the refinement calculation: 88 A-form backbone torsion angle constraints were added for the nucleotides in both stems. Adding the A-form restraints did not change the global shape of the molecules; it only lowered the root mean square deviation (r.m.s.d.) among the 12 acceptable structures. The refined structures were subjected to a final energy minimization calculation. The calculated structures were judged by monitoring their NOE violations; none of the final structures had any individual distance constraint violation >0.2 Å.

Figure 5 shows a view of 12 converged structures superimposed on the basis of all atoms. For clarity only the phosphate backbones of the molecules are shown to represent the overall conformation of the pseudoknot APKA27G. The superimposition of both stems is fairly good, although superimposition of the loops is relatively poor. The precision of the structures was evaluated by calculating their r.m.s.d. for all atoms relative to the averaged structure. The

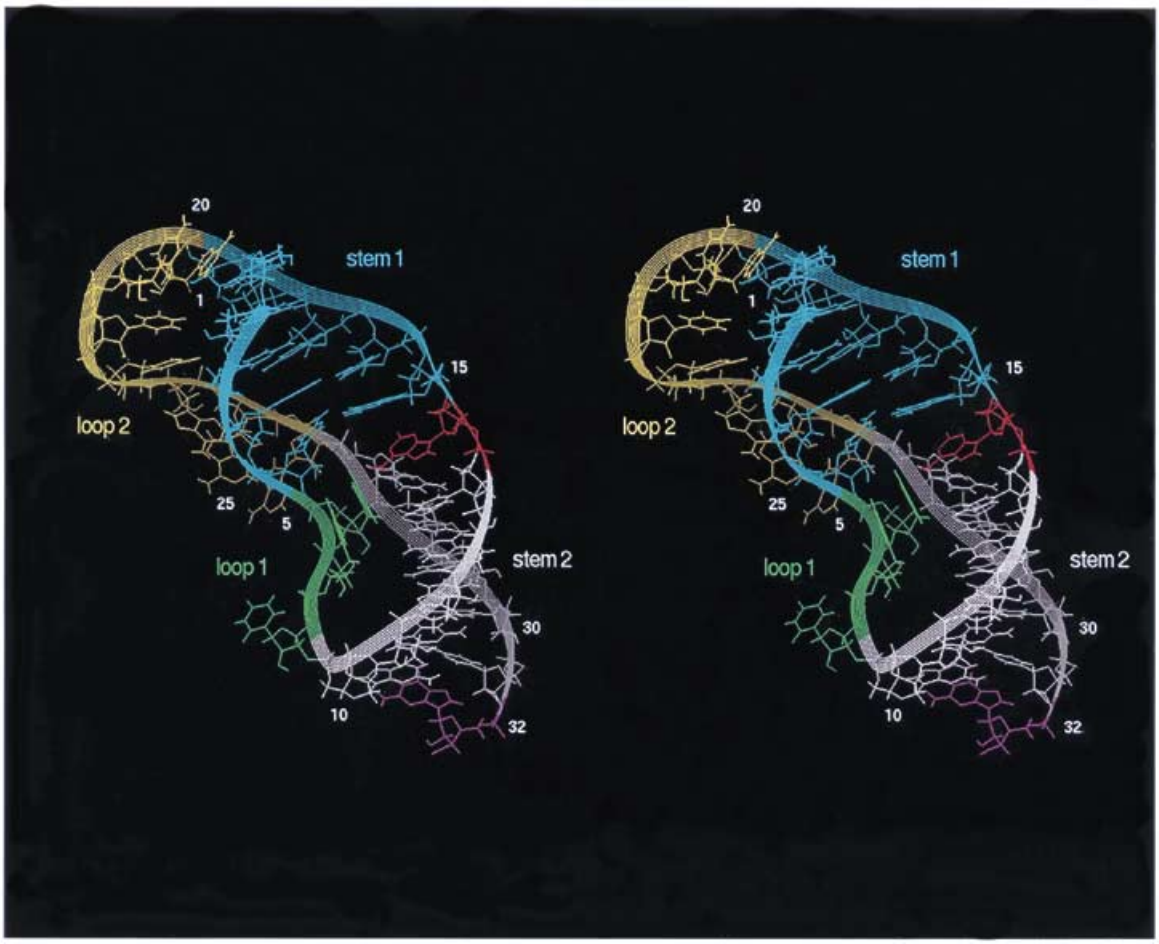

Figure 6. Stereo view of the averaged structure of pseudoknot APKA27G. The stems and loops are colored differently so that four regions of the molecule can be distinguished. One unpaired intervening nucleotide (red) is stacked between stem 1 (blue) and stem 2 (white). The two stems are not coaxial, but are bent relative to each other. Loop 1 (green) crosses the deep major groove of stem 2 and loop 2 (yellow) crosses the shallow minor groove of stem 1.

average r.m.s.d. for the 12 structures was 2.5 Å. The overall conformation of the pseudoknot APKA27G is different from that of the parent pseudoknot APK, but is similar to that of the efficient frameshifting pseudoknot VPK (6). The pseudoknot is not straight, but bent. To calculate the angle between the two stems of the pseudoknot, the helix axes for the two stems were generated using the program NEWHEL93 (R.E.Dickerson, University of California, Los Angeles, CA). The bending angle between the two stems of the pseudoknot APKA27G was ~132° (±4°).

A detailed picture of the average pseudoknot structure is shown in Figure 6. The phosphate backbone from G9 to A20 is a continuous A-form helix with a small perturbation at the junction of stems 1 and 2. On the opposite strand, the two stem regions (G1–C5 and G27–C31) are stacked in A-form geometry. The U13·G27 base pair does form, unlike APK, where no U13·A27 base pair forms. In contrast to the two intervening nucleotides observed for APK, a single adenylate residue intervenes between the two stems and interrupts coaxial stacking of the stems. This unpaired residue serves as a hinge to cause the pseudoknot to bend from a linear conformation. Loop 1 crosses the deep major groove of stem 2 and loop 2 crosses the minor groove of stem 1, as observed for other pseudoknots with right handed coaxial stacking of their stems (6,21,22).

DISCUSSION

One striking difference in the secondary structure between the mutant pseudoknot APKA27G and the parent pseudoknot APK is that in the mutant the U13·G27 base pair does form in stem 2, in contrast to the lack of formation of the corresponding U13·A27 base pair in the parent pseudoknot. This different base pairing may be due to the more favorable stacking interaction between G27 and G28 in the mutant pseudoknot than that of A27 and G28 in the parent pseudoknot. This extra base pair at the top of stem 2 leaves only one nucleotide at the junction of the two stems. This is a critical feature in determining the unique conformation of the pseudoknot. In a previous paper (7), we found that in APK two unpaired nucleotides between the two stems cause an open conformation in which the two stems are twisted relative to each other (7). Computer modeling showed that the conformation of APK could be dramatically changed and converted to a structure similar to the efficient frameshifting pseudoknot VPK by simply forcing the U13·A27 base pair to form at the top of stem 2.

Stacking interaction between nucleotides and sugar pucker conformation of the nucleotides in loop 2 are closely related to the proper orientation of loop 2 relative to stem 1. Since G27 in the mutant pseudoknot APKA27G is involved in the formation of a

base pair in stem 2, APKA27G has one less nucleotide in loop 2 compared with pseudoknots APK and VPK. Therefore, nucleotides in loop 2 must adopt a more extended conformation to bridge the minor groove of stem 1. This is clearly indicated by the NMR data, showing that the loop nucleotides adopt a C2′-*endo* sugar conformation, resulting in a distance of ~7 Å between neighboring phosphate groups (17), instead of a C3′-*endo* or mixture of C2′- and C3′-*endo* pucker as observed in APK and VPK. In addition, less stacking interactions between nucleotides in loop 2 of APKA27G compared with those of APK or VPK also contribute to the extended conformation of loop 2.

The efficient frameshifting RNA pseudoknots all adopt common structural features. The mutant RNA pseudoknot APKA27G is very similar in conformation to other frameshifting pseudoknots, VPK and U13C (6,8). The common structural features of the efficient frameshifting pseudoknots are that coaxial stacking of the two stems is interrupted by an intervening nucleotide that causes a bend between the two stems. All three pseudoknots have similar bends in which stem 1 bends towards loop 1, which crosses the major groove of stem 2. This unique conformation of the pseudoknot may be required for recognition by ribosome or ribosome-related factors during translation of viral mRNA. The fact that conformation not sequence is the dominant requirement for frameshifting is strengthened by the fact that sequences of base pairs in the stems (1–5) or sequences of bases in loop 2 (Prof. Raymond Gesteland, personal communication) do not have a large effect on frameshifting.

The thermodynamic stability of a pseudoknot is considered to be a major factor for promoting efficient frameshifting in retroviruses. Thus the increase in frameshifting efficiency by mutant pseudoknot APKA27G over the parent pseudoknot APK might be due to the higher stability of APKA27G. Although APKA27G contains one more base pair at the end of stem 2 than APK, this G·U base pair is not very stable, as indicated by the fast exchange of the U13 imino proton with the solvent. UV melting studies also indicate that the melting temperature (64°C) of the mutant pseudoknot is not increased compared with that of the parent pseudoknot. Thus the higher frameshifting ability of the mutant pseudoknot APKA27G cannot be attributed to increased thermodynamic stability.

Comparison of the structures and frameshifting abilities of the mutant pseudoknot APKA27G and the parent pseudoknot APK illustrates the sensitvity of the structure and function of RNA to small changes in sequence. In the mutant pseudoknot APKA27G a single A→G substitution changes its structure and greatly increases its frameshifting efficiency. This further supports the hypothesis of a specific structure-dependent frameshifting process in retroviruses.

ACKNOWLEDGEMENTS

We thank Ms Barbara Dengler for general assistance and Mr David Koh for synthesizing DNA templates. H.K. was supported by a post-doctoral fellowship from the Program in Mathematics and Molecular Biology, which is supported by the National Science Foundation. This research was supported in part by National Institute of Health grant GM 10840, by Department of Energy grant DE-FG03-86ER60406 and through instrumentation grants from the Department of Energy (DE-FG05-86ER75281) and the National Science Foundation (DMB 86-09305).

REFERENCES

1 Atkins,J.F., Weiss,R.B. and Gesteland,R.F. (1990) *Cell*, **62**, 413–423.
2 Jacks,T. (1990) *Curr. Topics Microbiol. Immunol.*, **157**, 93–124.
3 Tu,C., Tzeng,T.-H. and Bruenn,J.A. (1992) *Proc. Natl. Acad. Sci. USA*, **89**, 8636–8640.
4 Somogyi,P., Jenner,A.J., Brierley,I. and Inglis,S.C. (1993) *Mol. Cell. Biol.*, **13**, 6931–6940.
5 Chen,X., Chamorro,M., Lee,S.I., Shen,L.X., Hines,J.V., Tinoco,I. and Varmus,H.E. (1995) *EMBO J.*, **14**, 842–852.
6 Shen,L.X. and Tinoco,I. (1995) *J. Mol. Biol.*, **247**, 963–978.
7 Kang,H., Hines,J.V. and Tinoco,I. (1996) *J. Mol. Biol.*, **259**, 135–147.
8 Chen,X., Kang,H., Shen,L.X., Chamorro,M., Varmus,H.E. and Tinoco,I. (1996) *J. Mol. Biol.*, **260**, 479–483.
9 Milligan,J.F., Groebe,D.R., Witherell,G.W. and Uhlenbeck,O.C. (1987) *Nucleic Acids Res.*, **15**, 8783–8798.
10 Wyatt,J.R., Chastain,M. and Puglisi,J.D. (1991) *BioTechniques*, **11**, 764–769.
11 Wyatt,J.R., Puglisi,J.D. and Tinoco,I.,Jr (1990) *J. Mol. Biol.*, **214**, 455–470.
12 Plateau,P. and Guéron,M. (1982) *J. Am. Chem. Soc.*, **104**, 7310–7311.
13 Marion,D. and Wüthrich,K. (1983) *Biochem. Biophys. Res. Commun.*, **113**, 967–974.
14 Müller,N., Ernst,R.R. and Wüthrich,K. (1986) *J. Am. Chem. Soc.*, **108**, 6482–6492.
15 Shaka,A.J., Barker,P.B. and Freeman,R. (1985) *J. Magn. Resonance*, **64**, 547–552.
16 Bax,A. and Davis,D.G. (1985) *J. Magn. Resonance*, **65**, 355–360.
17 Saenger, W. (1984) In Cantor,C.R. (ed.), *Principles of Nucleic Acid Structure*. Springer-Verlag, New York, NY, pp. 256–261.
18 Brünger,A.T. (1992) *X-PLOR Version 3.0.* Yale University Press, New Haven, CT.
19 Wimberly,B. (1992) PhD thesis, University of California, Berkeley, CA.
20 Heus,H.A. and Pardi,A. (1991) *J. Am. Chem. Soc.*, **113**, 4360–4361.
21 Puglisi,J.D., Wyatt,J.R. and Tinoco,I.,Jr (1990) *J. Mol. Biol.*, **214**, 437–453.
22 Pleij,C.W.A., Rietveld,K. and Bosch,L. (1985) *Nucleic Acids Res.*, **13**, 1717–1731.